ARTICLES SCIENCE CHINA Materials

mater.scichina.com link.springer.com

Published online 16 May 2018 | 10.1007/s40843-018-9288-4
Sci China Mater 2019, 62(1): 130–137

Mn^{2+}-activated calcium fluoride nanoprobes for time-resolved photoluminescence biosensing

Jiaojiao Wei[1,2], Wei Zheng[1,2*], Xiaoying Shang[1], Renfu Li[1], Ping Huang[1], Yan Liu[1], Zhongliang Gong[1], Shanyong Zhou[1], Zhuo Chen[1] and Xueyuan Chen[1,2*]

ABSTRACT **Time-resolved (TR) photoluminescence (PL) technique has shown great promise in ultrasensitive biodetection and high-resolution bioimaging. Hitherto, almost all the TRPL bioprobes are based on the parity-forbidden f→f transition of lanthanide ions. Herein, we report TRPL biosensing by taking advantage of the d→d transition of transition metal (TM) Mn^{2+} ion. We demonstrate that the Förster resonance energy transfer (FRET) signal can be distinguished from that of radiative reabsorption process through measuring the PL lifetime of Mn^{2+}, thus establishing a reliable method for Mn^{2+} in homogeneous TR-FRET biodetection. We also demonstrate the biotin receptor-targeted cancer cell imaging by utilizing biotinylated CaF_2:Ce,Mn nanoprobes. Furthermore, we show in a proof-of-concept experiment the application of the long-lived PL of Mn^{2+} for TRPL bioimaging through the burst shot with a cell phone. These findings provide a general approach for exploiting the long-lived PL of TM ions for TRPL biosensing, thereby opening up a new avenue for the exploration of novel and versatile applications of TM ions.**

Keywords: manganese, time-resolved photoluminescence, energy transfer, biodetection, bioimaging

INTRODUCTION

Time-resolved (TR) photoluminescence (PL) technique has shown great promise in ultrasensitive biodetection and high-resolution bioimaging, owing to its ability to eliminate the short-lived background noise from biological autofluorescence and scatter light (in the nanosecond range) by setting a temporal delay in signal acquisition [1–5]. Hitherto, almost all the TRPL bioprobes are based on lanthanide chelates or lanthanide-doped nanoparticles (NPs), by taking advantage of the long-lived PL (μs–ms range) of lanthanide ions originating from the parity-forbidden intra-$4f^N$ electronic transition [6–10]. In addition to lanthanide ions, the forbidden d→d transition of transition metal (TM) ions such as Mn^{2+} with d^5 configuration results in a long PL lifetime ranging from microseconds to tens of milliseconds [11–15]. The long PL lifetime of Mn^{2+} ions makes it a potential bioprobe in TRPL biosensing, which, however, has scarcely been reported [16].

Mn^{2+}-activated luminescent materials typically possess a broad emission band varying from green to deep red depending on the crystal field of Mn^{2+} [17]. For example, the octahedrally coordinated Mn^{2+} in CaF_2 lattice display green emission with a long PL lifetime up to tens of milliseconds [18–20]. Such long-lived and broad-band PL of Mn^{2+} along with the excellent biocompatibility of CaF_2 is desirable for homogeneous TR Förster resonance energy transfer (FRET) biodetection [21–24]. The broad emission band of Mn^{2+} enhances spectral overlap with the excitation band of the energy acceptor, resulting in an enhanced FRET efficiency [25–28]. Nonetheless, the reabsorption process, which is unavoidable in homogeneous luminescent bioassays, may interfere with the FRET signal and lead to incorrect detection results [29–31]. Therefore, it is of fundamental importance to gain deep insights into the energy transfer process and establish a reliable method for Mn^{2+} in homogeneous TR-FRET biodetection.

Herein, we report the application of CaF_2:Ce,Mn NPs for TRPL biodetection and bioimaging by utilizing the long-lived PL of Mn^{2+}. We demonstrate that the PL lifetime of Mn^{2+} can be exploited as a distinguishable FRET signal for Mn^{2+} in TR-FRET biodetection based on the energy transfer between the NP donor and organic dye

[1] CAS Key Laboratory of Design and Assembly of Functional Nanostructures, State Key Laboratory of Structural Chemistry, and Fujian Key Laboratory of Nanomaterials, Fujian Institute of Research on the Structure of Matter, Chinese Academy of Sciences, Fuzhou 350002, China
[2] College of Materials Science and Engineering, Fujian Normal University, Fuzhou 350007, China
* Corresponding authors (emails: zhengwei@fjirsm.ac.cn (Zheng W); xchen@fjirsm.ac.cn (Chen X))

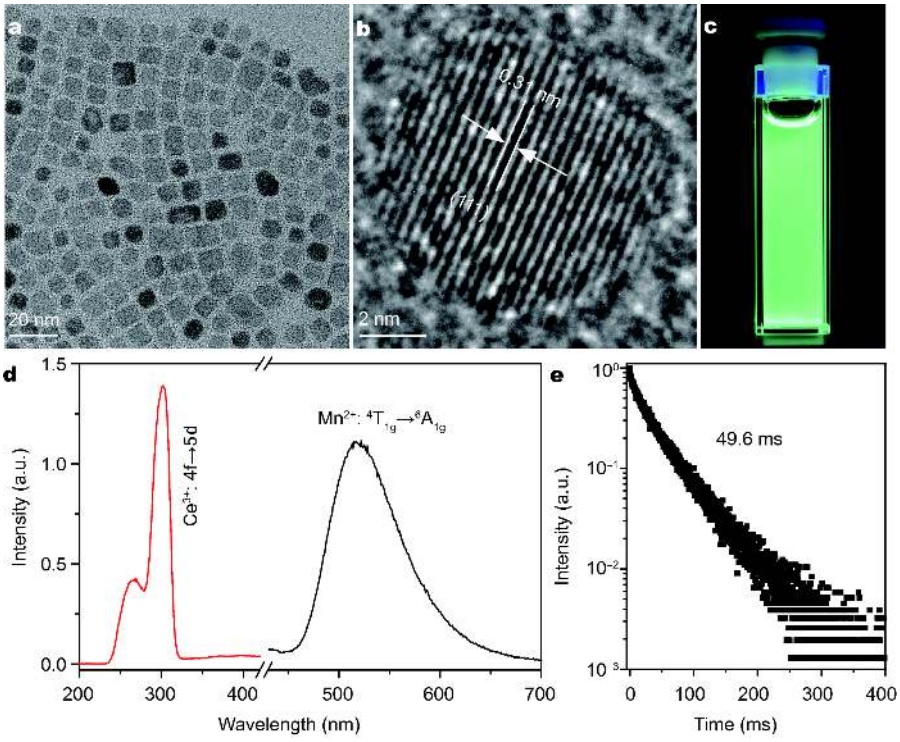

Figure 1 (a) TEM and (b) HRTEM images of CaF_2:5%Ce,5%Mn NPs. (c) PL photograph of the NPs dispersed in cyclohexane under 304-nm UV lamp irradiation. (d) PL emission spectrum (black) of CaF_2:5%Ce,5%Mn NPs upon UV excitation at 304 nm, and their excitation spectrum (red) by monitoring the Mn^{2+} emission at 520 nm. (e) PL decay from $^4T_{1g}$ by monitoring the Mn^{2+} emission at 520 nm.

acceptor in an avidin/biotin model system. We also demonstrate the biotin receptor-targeted cancer cell imaging by biotinylated CaF_2:Ce,Mn NPs as luminescent nanoprobes. Furthermore, we propose a convenient and versatile method, namely, the burst shot with a cell phone for TRPL bioimaging of zebrafish fed with the nanoprobes, thereby revealing the great potential of the forbidden d→d transition of TM ions in TRPL biosensing.

RESULTS AND DISCUSSION

Monodisperse CaF_2:Ce,Mn NPs were synthesized through a solvothermal method in the presence of oleic acid as the surfactant and sodium ions as the codopant [32,33]. The as-synthesized NPs were hydrophobic and can be readily dispersed in nonpolar organic solvents such as cyclohexane. TEM image showed that the NPs were roughly cubic with an average length of 6.0±1.1 nm (Fig. 1a and Fig. S1a). High-resolution TEM image and XRD pattern confirmed the cubic phase and high crystallinity of the resulting NPs (Fig. 1b and Fig. S1b). Compositional analysis by EDS and ICP revealed the elements of Ca, F, Ce, Mn, and Na in the NPs (Fig. S1c and Table S1).

To achieve efficient PL in CaF_2:Ce,Mn NPs, the nominal dopant concentrations of Ce^{3+} and Mn^{2+} were optimized to be 5 mol% and 5 mol%, respectively (Fig. S2). Upon UV excitation at 304 nm, bright green PL of the colloidal NPs can be explicitly observed in cyclohexane solution (Fig. 1c). PL emission spectrum showed a broad emission band centered at 520 nm (Fig. 1d), which can be assigned to the spin-forbidden $^4T_{1g}(G) \rightarrow {}^6A_{1g}(S)$ transition of Mn^{2+} occupying an octahedral site (O_h) in CaF_2 lattice [18]. By monitoring the Mn^{2+} emission at 520 nm, two broad excitation bands centered at 260 nm and 304 nm were detected. The excitation band at 304 nm can be assigned to the 4f→5d transition of Ce^{3+} in C_{4v} center, indicating an energy transfer from Ce^{3+} to Mn^{2+} [19]. The excitation band at 260 nm is associated with the Ce^{3+} transitions in clusters (Fig. S3) [20]. The PL decay from $^4T_{1g}$ indicates an ultralong effective PL lifetime of 49.6 ms for the Mn^{2+} emission (Fig. 1e and Table S2), typical of the forbidden d→d transition within Mn^{2+} ions [17].

For bioapplications, we rendered the hydrophobic CaF_2:Ce,Mn NPs to be hydrophilic and biocompatible by removing the oleate ligands from their surface through an acid-washing treatment [34], which was confirmed by Fourier transform infrared (FTIR) spectra and thermo-

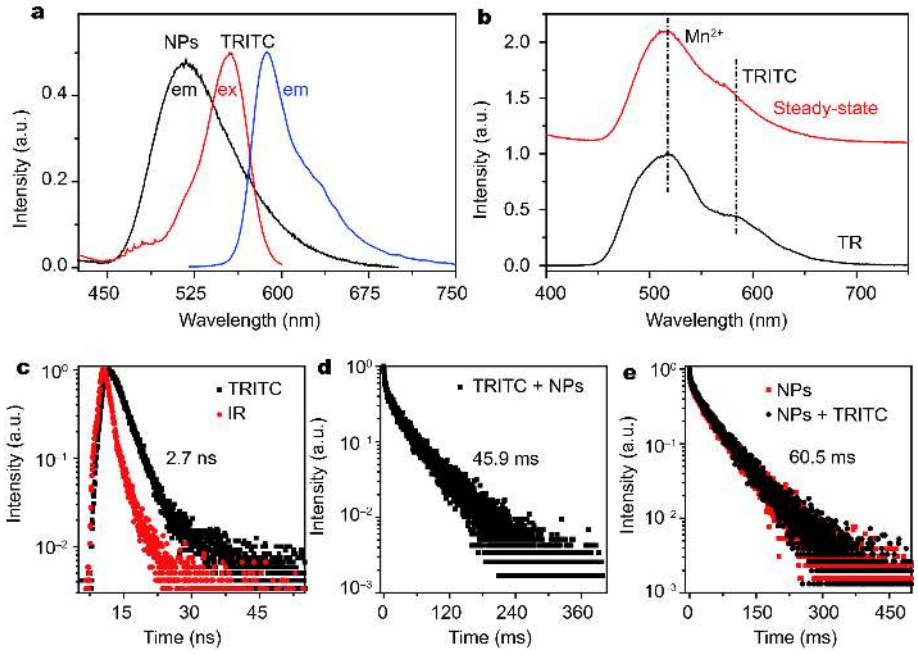

Figure 2 (a) PL emission spectrum of CaF_2:5%Ce,5%Mn NPs (black); excitation (red) and emission (blue) spectra of TRITC. (b) Steady-state and TRPL (delay time=100 μs, gate time=5 ms) emission spectra for the aqueous solution containing 50 μmol L^{-1} of PAA-capped NPs and 10 nmol L^{-1} of TRITC upon UV excitation at 304 nm. (c) PL decays of TRITC by monitoring its emission at 650 nm upon excitation with a 397-nm nanosecond pulsed laser. IR denotes the instrument response. (d) PL decay of the NPs-TRITC mixture by monitoring the TRITC emission at 650 nm under excitation at 304 nm. (e) PL decays of PAA-capped NPs (black) and NPs-TRITC mixture (red) by monitoring the Mn^{2+} emission at 520 nm under excitation at 304 nm.

gravimetric analysis (TGA) for NPs before and after acid-washing treatment (Figs S4, S5). As a result, these ligand-free NPs exhibited well water solubility. More importantly, we found that the integrated PL intensity of ligand-free NPs was enhanced by a factor of 3.1 relative to their oleate-capped counterparts, with their PL lifetime increasing from 49.6 ms to 59.5 ms (Fig. S6). Accordingly, the absolute PL quantum yield, defined as the ratio of the number of emitted photons to the number of absorbed photons, was determined to increase remarkably from 15.3±0.8% in oleate-capped NPs to 37.0±2.3% in ligand-free NPs, which is attributed to the increased absorption of the excitation light by Ce^{3+} followed by energy transfer to Mn^{2+} [35]. The long PL lifetime is probably due to the change of refractive index of the surrounding medium, which changed the radiative decay rate of Mn^{2+}, as well documented in $LaPO_4$:Ce/Tb NPs with nanocrystal-cavity model proposed by Meijerink *et al.* [36].

Due to the removal of surface ligands, positively charged Ca^{2+} ions were exposed on the surface of ligand-free NPs, endowing the NPs with a zeta potential of +48.2 mV at pH 6.9. As a consequence, these ligand-free NPs are allowed for direct conjugation with electronegative groups of hydrophilic and biocompatible molecules such as biotin and poly(acrylic acid) (PAA) through the strong chelation of Ca^{2+} [37,38]. The conjugation of biotin and PAA to the NP surface was confirmed by FTIR spectra, TGA, dynamic light scattering and zeta potential measurements (Figs S4, S5, and S7). The PAA-capped NPs and biotinylated NPs preserved the intense PL of ligand-free NPs with PL lifetimes of 60.5 ms and 54.1 ms, respectively (Fig. S6 and Table S2).

To validate the feasibiliy of the long-lived and broadband PL of Mn^{2+} for homogeneous TR-FRET biodetection, we selected CaF_2:Ce,Mn NPs and tetramethylrhodamine B isothiocyanate (TRITC) as the energy donor and acceptor, respectively, in view of the large spectral overlap between the emission band of the NPs (450–700 nm) and the excitation band of TRITC (450–600 nm) (Fig. 2a). Fig. 2b compares the steady-state with TRPL emission spectra for the aqueous solution containing 50 μmol L^{-1} of PAA-capped NPs and 10 nmol L^{-1} of TRITC upon UV excitation at 304 nm, which show similar emission bands from 450 to 700 nm consisting of both Mn^{2+} and TRITC emissions. The steady-state PL emissions of Mn^{2+} and TRITC were attributed to direct excitation of the NPs and TRITC by the 304-nm UV light (Fig. S8). In the TRPL spectrum, the intrinsic short-lived PL (2.7 ns) of TRITC

arising from direct excitation (Fig. 2c) was eliminated by setting a delay time of 100 μs. Thus, the long-lived PL of TRITC in the TRPL spectrum was ascribed to the energy transfer from the NPs to TRITC (Fig. S9), which caused the longer PL lifetime of TRITC from 2.7 ns to 45.9 ms due to the slow population of the TRITC excited state from the long-lived Mn^{2+} excited state (Fig. 2d) [25]. Because no specific binding between PAA-capped NPs and TRITC could bring them within effective FRET distance [39], we deduced that the NPs-to-TRITC energy transfer is governed by a radiative reabsorption process rather than a non-radiative FRET process. Such radiative energy transfer was further evidenced by the identical PL lifetime of Mn^{2+} in either NPs-TRITC mixture or pure PAA-capped NPs (Fig. 2e), since non-radiative FRET always results in a decrease in PL lifetime of energy donor by imposing additional relaxation channel on the donor [40]. These results unveil that the radiative energy transfer from long-lived energy donor to short-lived energy acceptor is able to lengthen the PL lifetime of the acceptor. Note that this is the first demonstration on PL lifetime lengthening of short-lived energy acceptor by long-lived donor through radiative reabsorption process, which is very important in homogeneous luminescent bioassays.

By employing biotinylated CaF_2:Ce,Mn NPs and TRITC-labelled avidin, we constructed the FRET pair in an avidin/biotin model system, in which the excitation energy was transferred from the NPs to nearby TRITC through either radiative reabsorption or FRET as a result of specific binding between avidin and biotin [38]. For non-binding control, we used PAA-capped NPs as the energy donor under otherwise identical conditions, whereby the radiative reabsorption process was the only energy transfer route (Fig. 3a). Because both the radiative reabsorption and FRET processes can lengthen the PL lifetime of TRITC (Fig. S10), the Mn^{2+} and TRITC emissions were detected in the TRPL spectra for either biotinylated or PAA-capped NPs incubated with TRITC-labelled avidin, yielding nearly identical emission patterns (Fig. 3b, c). As a result, the FRET signal was undistinguishable and submerged in the TRPL signal arising from radiative reabsorption, which makes the TRPL spectrum unreliable for homogeneous TR-FRET biodetection.

We measured the PL lifetime of the energy donor to distinguish the FRET signal from that of the radiative reabsorption process. Fig. 3d shows the concentration-dependent PL lifetimes of Mn^{2+} in the mixture of biotinylated NPs and TRITC-labelled avidin. It was found that the PL lifetime of Mn^{2+} in biotinylated NPs decreased from 54.1 to 26.4 ms as the avidin concentration increased from 0 to 588 nmol L^{-1}, as a result of FRET from the NPs to TRITC. By contrast, in non-binding control, the PL lifetime of Mn^{2+} in PAA-capped NPs showed only a slight decrease at high avidin concentrations, attributed to non-specific binding between PAA-capped NPs and TRITC-labelled avidin, which can be avoided by blocking the residual active binding site of PAA-capped NPs for avidin through surface modification. This enables us to quantify the avidin concentration by measuring the PL lifetime of Mn^{2+} (Fig. 3f). The detection limit, defined as the concentration that corresponds to 3 times the standard deviation below the signal measured in the blank control, was determined to be 32 pmol L^{-1}. This value is approximately one order of magnitude improvement relative to that in TR-FRET assays based on lanthanide-doped nanoprobes ever reported [33]. These results show that the PL lifetime of Mn^{2+} is sensitive to FRET and barely affected by the radiative reabsorption process, thus validating its reliability and advantages in TR-FRET bioassay.

Utilizing biotinylated CaF_2:Ce,Mn NPs, we also demonstrated biotin receptor-targeted cancer cell imaging. Biotin is a growth promoter at the cellular level, and biotin receptors are overexpressed in many cancer cells, including colon (Colo-26), lung (M109), renal (RD0995), ovarian (Ov2008) and cervical (HeLa) cancer cell lines [41,42]. We selected HeLa cells with biotin receptors overexpressed on the membrane as the target cancer cells and human normal liver (L-02) cells with low-expressed biotin receptors as the control. Owing to the high affinity between biotin and biotin receptors, biotinylated NPs can specifically target to HeLa cells, leading to bright green PL (green channel) of Mn^{2+} surrounding HeLa cells (Fig. 4a). By contrast, the green PL of Mn^{2+} was hardly observed on L-02 cells under otherwise identical conditions due to the lack of specific recognition between biotinylated NPs and L-02 cells (Fig. 4b). MTT assay on L-02 cells incubated with biotinylated NPs showed a cell viability larger than 95% even at a high NP concentration of 1 mg mL^{-1} (Fig. S11), indicating that biotinylated CaF_2:Ce,Mn NPs are biocompatible and nontoxic to live cells. Our results show that CaF_2:Ce,Mn NPs modified with specific capture molecules, like biotin for biotin receptor, can be used as effective luminescent nano-bioprobes for targeted tumor imaging.

Furthermore, by means of the camera burst mode on a cell phone [43], we demonstrated in a proof-of-concept experiment the application of CaF_2:Ce,Mn nanoprobes

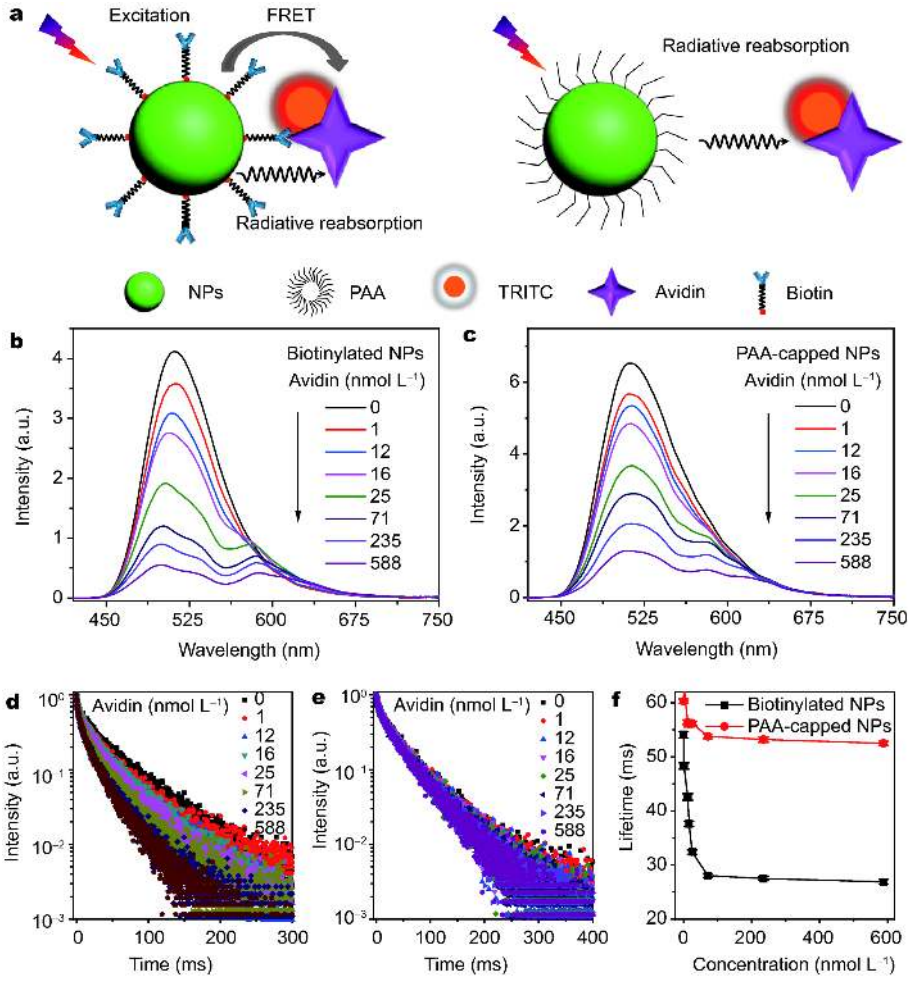

Figure 3 (a) Schematic illustration of the energy transfer processes between CaF_2:Ce,Mn NPs and TRITC in cases of specific binding (left) and non-specific binding (right). TRPL spectra of (b) biotinylated and (c) PAA-capped CaF_2:Ce,Mn NPs incubated with TRITC-labeled avidin as a function of the avidin concentration. PL decays from (d) biotinylated and (e) PAA-capped CaF_2:Ce,Mn NPs at different avidin concentrations by monitoring the Mn^{2+} emission at 520 nm. (f) Effective PL lifetime of $^4T_{1g}$ of Mn^{2+} as a function of the avidin concentration, as obtained from (d, e). Each PL lifetime was measured independently for three times to yield the average value and standard deviation.

for TRPL bioimaging. The fast burst mode on HUAWEI P10 cell phone is able to continuously capture 10 photos in 1 s with an exposure time of 0.1 s for each photo. Fig. 5a compares the PL photographs for the aqueous solution of ligand-free NPs and TRITC, respectively. The NPs and TRITC solution displayed bright green and orange PL, respectively, under 304-nm UV lamp irradiation. When the lamp was off, the TRITC PL vanished immediately in the photos captured by the camera due to the short-lived PL (~2.7 ns) of TRITC. By contrast, the green PL of Mn^{2+} can last for ~400 ms and remained explicitly visualized in the first four photos after the lamp was off. This suggests that the cell phone can be explored as a convenient and efficient detector to capture the long-lived PL of Mn^{2+} for TRPL bioimaging. To demonstrate this concept, we carried out steady-state and TRPL imaging of 5-day-old zebrafish after feeding it with ligand-free CaF_2:Ce,Mn NPs through burst shot with the cell phone. In the steady-state PL image when the lamp was on, the green PL was observed in both the zebrafish and the background, whereas in the TRPL image when the lamp was off, the green PL was observed exclusively in the zebrafish (Fig. 5b), confirming that the PL signal in the zebrafish originated from the digested CaF_2:Ce,Mn NPs. These results verify that the TRPL technique based on the long-lived PL of Mn^{2+} can effectively suppress the short-lived background noise and offer improved imaging sensitivity relative to that of steady-state PL. Along with the large longitudinal magnetic relaxivity of Mn^{2+} (Fig. S12), these CaF_2:Ce,Mn NPs may function as TRPL/MRI dual-mode

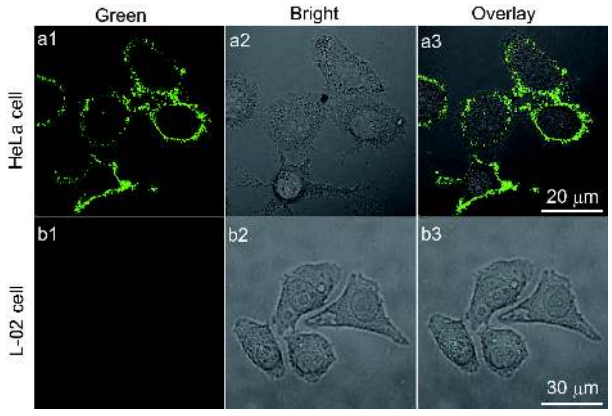

Figure 4 Confocal laser scanning microscopy images of (a1–a3) HeLa cells and (b1–b3) L-02 cells after incubation with biotinylated CaF_2:Ce,Mn NPs (0.5 mg mL^{-1}) at 37°C for 2 h. Intense green PL of Mn^{2+} (λ_{em}=500–560 nm, λ_{ex}=408 nm) was observed exclusively in HeLa cells. Panel 1 and 2 show the green PL images and bright-field images, respectively. Panel 3 is the overlay images of panels 1 and 2.

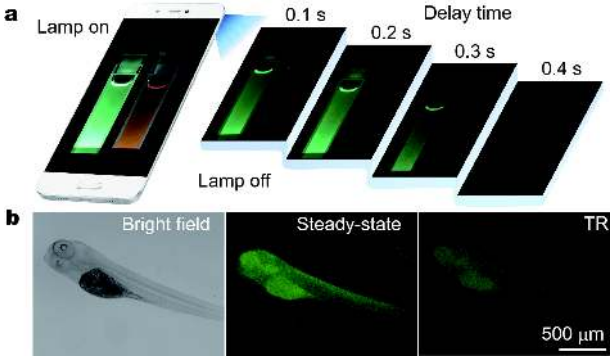

Figure 5 (a) Schematic representation of the camera burst mode on a cell phone. The image in the cell phone represents the steady-state PL photo for the aqueous solution of ligand-free CaF_2:Ce,Mn NPs (left) and TRITC (right) under 304-nm UV lamp irradiation. The images outside the cell phone denote the corresponding TRPL photos of the NPs and TRITC, captured by the cell phone in sequence with a time interval of 0.1 s. (b) Microscopic bright field, steady-state and TRPL images of the 5-day-old zebrafish fed with ligand-free CaF_2:Ce,Mn NPs (0.5 mg mL^{-1}).

nano-bioprobes. It is worthy of mentioning that, these CaF_2:Ce,Mn NPs are more suitable for *in-vitro* biodetection and bioimaging than *in-vivo* applications due to the shallow tissue penetration depth of visible light.

CONCLUSIONS

In summary, we have demonstrated the advantages of CaF_2:Ce,Mn NPs as TRPL nano-bioprobes for sensitive biodetection and high-resolution bioimaging based on the long-lived PL of Mn^{2+}. Our mechanistic investigation on the energy transfer processes revealed that the FRET signal can be distinguished from that of reabsorption process by measuring the PL lifetime of Mn^{2+} instead of the TRPL spectrum, thus establishing a reliable tool for homogeneous TR-FRET bioassay. The proposed burst shot with a cell phone can effectively capture the long-lived PL of Mn^{2+}, providing a convenient and versatile approach for TRPL bioimaging without the need of a sophisticated instrument. These findings offer new routes to the development of ultrasensitive TRPL biosensing by exploiting the forbidden d→d transitions of TM ions, thereby opening up a new avenue for clinical applications, such as *in-vitro* detection and targeted cancer imaging.

Received 28 March 2018; accepted 24 April 2018; published online 16 May 2018

1 Siitari H, Hemmilä I, Soini E, *et al.* Detection of hepatitis B surface antigen using time-resolved fluoroimmunoassay. Nature, 1983, 301: 258–260
2 Connally RE, Piper JA. Time-gated luminescence microscopy. Ann New York Acad Sci, 2008, 1130: 106–116
3 Jin D, Piper JA, Leif RC, *et al.* Time-gated flow cytometry: an ultra-high selectivity method to recover ultra-rare-event μ-targets in high-background biosamples. J Biomed Opt, 2009, 14: 024023
4 Zheng W, Tu D, Huang P, *et al.* Time-resolved luminescent biosensing based on inorganic lanthanide-doped nanoprobes. Chem Commun, 2015, 51: 4129–4143
5 Song B, Ye Z, Yang Y, *et al.* Background-free *in-vivo* imaging of vitamin C using time-gateable responsive probe. Sci Rep, 2015, 5: 14194
6 Bünzli JCG, Piguet C. Taking advantage of luminescent lanthanide ions. Chem Soc Rev, 2005, 34: 1048–1077
7 Yuan J, Wang G. Lanthanide-based luminescence probes and time-resolved luminescence bioassays. TrAC Trends Anal Chem, 2006, 25: 490–500
8 Bouzigues C, Gacoin T, Alexandrou A. Biological applications of rare-earth based nanoparticles. ACS Nano, 2011, 5: 8488–8505
9 Huang P, Tu D, Zheng W, *et al.* Inorganic lanthanide nanoprobes for background-free luminescent bioassays. Sci China Mater, 2015, 58: 156–177
10 Zheng W, Zhou S, Xu J, *et al.* Ultrasensitive luminescent *in vitro* detection for tumor markers based on inorganic lanthanide nano-bioprobes. Adv Sci, 2016, 3: 1600197
11 Klick CC, Schulman JH. On the luminescence of divalent manganese in solids. J Opt Soc Am, 1952, 42: 910–916
12 He Y, Wang HF, Yan XP. Exploring Mn-doped ZnS quantum dots for the room-temperature phosphorescence detection of enoxacin in biological fluids. Anal Chem, 2008, 80: 3832–3837
13 Zhao Q, Huang C, Li F. Phosphorescent heavy-metal complexes for bioimaging. Chem Soc Rev, 2011, 40: 2508–2524
14 Deng X, Dai Y, Liu J, *et al.* Multifunctional hollow CaF_2:Yb^{3+}/Er^{3+}/Mn^{2+}-poly(2-Aminoethyl methacrylate) microspheres for Pt(IV) pro-drug delivery and tri-modal imaging. Biomaterials, 2015, 50: 154–163
15 Liu X, Wang Y, Li X, *et al.* Binary temporal upconversion codes of Mn^{2+}-activated nanoparticles for multilevel anti-counterfeiting. Nat Commun, 2017, 8: 899

16 Zhu D, Chen Y, Jiang L, *et al.* Manganese-doped ZnSe quantum dots as a probe for time-resolved fluorescence detection of 5-fluorouracil. Anal Chem, 2011, 83: 9076–9081
17 Blasse G, Grabmaier BC. Luminescent Materials. Berlin: Springer-Verlag, 1994
18 Alcalá R, Alonso PJ, Lalinde G, *et al.* Manganese centers in low temperature X-irradiated CaF_2:Mn. Phys Stat Sol b, 1980, 98: 315–322
19 McKeever SWS, Brown MD, Abbundi RJ, *et al.* Characterization of optically active sites in CaF_2:Ce,Mn from optical spectra. J Appl Phys, 1986, 60: 2505–2510
20 G UC. On the Ce–Mn clustering in CaF_2 in which the $Ce^{3+}\rightarrow Mn^{2+}$ energy transfer occurs. J Phys-Condens Matter, 2003, 15: 3821–3830
21 Lundin K, Blomberg K, Nordström T, *et al.* Development of a time-resolved fluorescence resonance energy transfer assay (cell tr-fret) for protein detection on intact cells. Anal Biochem, 2001, 299: 92–97
22 Wang L, Tan W. Multicolor FRET silica nanoparticles by single wavelength excitation. Nano Lett, 2006, 6: 84–88
23 Shen J, Sun LD, Zhu JD, *et al.* Biocompatible bright YVO_4:Eu nanoparticles as versatile optical bioprobes. Adv Funct Mater, 2010, 20: 3708–3714
24 Li Z, Zhang Y, Huang L, *et al.* Nanoscale "fluorescent stone": luminescent calcium fluoride nanoparticles as theranostic platforms. Theranostics, 2016, 6: 2380–2393
25 Kaiser U, Sabir N, Carrillo-Carrion C, *et al.* Förster resonance energy transfer mediated enhancement of the fluorescence lifetime of organic fluorophores to the millisecond range by coupling to Mn-doped CdS/ZnS quantum dots. Nanotechnology, 2016, 27: 055101
26 Qiao J, Xia Z, Zhang Z, *et al.* Near UV-pumped yellow-emitting $Sr_9MgLi(PO_4)_7:Eu^{2+}$ phosphor for white-light LEDs. Sci China Mater, 2018, 61: 985–992
27 Yu M, Qu Y, Pan K, *et al.* Enhanced photoelectric conversion efficiency of dye-sensitized solar cells by the synergetic effect of $NaYF_4:Er^{3+}/Yb^{3+}$ and g-C_3N_4. Sci China Mater, 2017, 60: 228–238
28 Wang D, Wang R, Liu L, *et al.* Down-shifting luminescence of water soluble $NaYF_4:Eu^{3+}$@Ag core-shell nanocrystals for fluorescence turn-on detection of glucose. Sci China Mater, 2017, 60: 68–74
29 Kochubey VI, Konyukhova YG, Zabenkov IV, *et al.* Accounting for scattering and reabsorption in the analysis of luminescence spectra of nanoparticles. Quantum Electron, 2011, 41: 335–339
30 Anni M, Alemanno E, Creti A, *et al.* Interplay between amplified spontaneous emission, Forster resonant energy transfer, and self-absorption in hybrid poly(9,9-dioctylfluorene)-CdSe/ZnS nanocrystal thin films. J Phys Chem A, 2010, 114: 2086–2090
31 Achatz DE, Meier RJ, Fischer LH, *et al.* Luminescent sensing of oxygen using a quenchable probe and upconverting nanoparticles. Angew Chem Int Ed, 2011, 50: 260–263
32 Wang G, Peng Q, Li Y. Upconversion luminescence of monodisperse $CaF_2:Yb^{3+}/Er^{3+}$ nanocrystals. J Am Chem Soc, 2009, 131: 14200–14201
33 Zheng W, Zhou S, Chen Z, *et al.* Sub-10 nm lanthanide-doped CaF_2 nanoprobes for time-resolved luminescent biodetection. Angew Chem Int Ed, 2013, 52: 6671–6676
34 Bogdan N, Vetrone F, Ozin GA, *et al.* Synthesis of ligand-free colloidally stable water dispersible brightly luminescent lanthanide-doped upconverting nanoparticles. Nano Lett, 2011, 11: 835–840
35 Chen X, Jin L, Sun T, *et al.* Energy migration upconversion in Ce (III)-doped heterogeneous core−shell−shell nanoparticles. Small, 2017, 13: 1701479
36 Senden T, Rabouw FT, Meijerink A. Photonic effects on the radiative decay rate and luminescence quantum yield of doped nanocrystals. ACS Nano, 2015, 9: 1801–1808
37 Huang P, Zheng W, Zhou S, *et al.* Lanthanide-doped $LiLuF_4$ upconversion nanoprobes for the detection of disease biomarkers. Angew Chem Int Ed, 2014, 53: 1252–1257
38 Zhou S, Zheng W, Chen Z, *et al.* Dissolution-enhanced luminescent bioassay based on inorganic lanthanide nanoparticles. Angew Chem Int Ed, 2014, 108: 12498–12502
39 Su Q, Feng W, Yang D, *et al.* Resonance energy transfer in upconversion nanoplatforms for selective biodetection. Acc Chem Res, 2017, 50: 32–40
40 Tu D, Liu L, Ju Q, *et al.* Time-resolved FRET biosensor based on amine-functionalized lanthanide-doped $NaYF_4$ nanocrystals. Angew Chem Int Ed, 2011, 50: 6306–6310
41 Russell-Jones G, McTavish K, McEwan J, *et al.* Vitamin-mediated targeting as a potential mechanism to increase drug uptake by tumours. J InOrg Biochem, 2004, 98: 1625–1633
42 Chen S, Zhao X, Chen J, *et al.* Mechanism-based tumor-targeting drug delivery system. Validation of efficient vitamin receptor-mediated endocytosis and drug release. Bioconjugate Chem, 2010, 21: 979–987
43 https://en.wikipedia.org/wiki/Burst_mode_(photography), Wikipedia

Acknowledgements This work is supported by National Program on Key Basic Research Project (973 Program, 2014CB845605), the Strategic Priority Research Program of the CAS (XDB20000000), the National Natural Science Foundation of China (21325104, 11774345, 21771185, 21501180 and 21650110462), the CAS/SAFEA International Partnership Program for Creative Re-search Teams, the Youth Innovation Promotion Association (2016277) and the Chunmiao Project of Haixi Institutes of the CAS (CMZX-2016-002), and Natural Science Foundation of Fujian Province (2017I0018 and 2017J05095).

Author contributions Wei J, Zheng W and Chen X conceived the project, wrote the paper and were primarily responsible for the experiments. Shang X and Li R carried out PL measurements. Huang P and Gong Z synthesized and characterized the NCs. Liu Y, Zhou S and Chen Z contributed to the TRPL biodetection and bioimaging. All authors contributed to the general discussion and revision of the manuscript.

Conflict of interest The authors declare no competing interests.

Supplementary information Experimental details and supporting data are available in the online version of the paper.

Jiaojiao Wei was born in Henan province of China. She is currently a master student in the College of Chemistry and Materials, Fujian Normal University, China. She joined Prof. Xueyuan Chen's group in Fujian Institute of Research on the Structure of Matter (FJIRSM), Chinese Academy of Sciences (CAS) in September 2016. She will graduate in June 2018. Her current research interest focuses on the controlled synthesis and optical spectroscopy of inorganic luminescent nanomaterials.

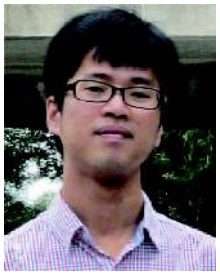

Wei Zheng earned his BSc degree (2007) in material forming and control engineering from Sichuan University and his PhD (2012) in Condensed Matter physics from FJIRSM, CAS. He joined Prof. Xueyuan Chen's group as a research assistant professor in September 2012 and was promoted to research associate professor in 2015. He joined the Youth Innovation Promotion Association of the CAS in 2016. Currently, his research interest focuses on the chemical synthesis, optical spectroscopy and bioapplications of inorganic luminescent nanomaterials.

Xueyuan Chen earned his BSc degree from the University of Science and Technology of China (1993) and his PhD degree from FJIRSM, CAS (1998). From 2001 to 2005, he was a postdoctoral research associate at the Chemistry Division of Argonne National Laboratory, U.S. Department of Energy, where he studied the photophysics and photochemistry of heavy elements. In 2005, he joined the faculty at FJIRSM, where he is currently a professor and group leader in Materials Chemistry and Physics. His research focuses on the chemistry, optical spectroscopy and bioapplications of lanthanide-doped luminescent nanomaterials.

基于Mn^{2+}激活氟化钙纳米荧光探针的时间分辨荧光生物分析

委娇娇[1,2], 郑伟[1,2*], 商晓颖[1], 李仁富[1], 黄萍[1], 刘奘[1], 宫仲亮[1], 周山勇[1], 陈卓[1], 陈学元[1,2*]

摘要 时间分辨荧光探测技术在超灵敏生物检测和高分辨生物成像领域具有广泛的应用前景.目前报道的时间分辨荧光生物探针大都是利用稀土离子$4f^N$电子组态间的禁戒跃迁发光. 本文报道了基于过渡金属Mn^{2+}离子d→d禁戒跃迁发光的时间分辨荧光生物分析. 我们证明通过测试Mn^{2+}的荧光寿命变化可以将荧光共振能量传递与辐射再吸收信号区分开来, 从而为Mn^{2+}发光在时间分辨荧光共振能量传递均相生物检测的应用提供了一种可靠的分析方法. 利用生物素化的CaF_2:Ce,Mn纳米荧光探针, 我们还实现了对生物素受体过表达癌细胞的靶向荧光成像. 通过概念性验证并利用手机连拍功能, 我们证明了Mn^{2+}的长寿命发光可用于时间分辨荧光生物成像. 这些研究结果为过渡金属长寿命发光在时间分辨荧光生物分析领域的应用提供了普适方法, 也为过渡金属离子的新型、多功能用途开辟了新的方向.

